PCCP

1H Chemical Shift Anisotropy: A High Sensitivity Solid-State NMR Dynamics Probe for Surface Studies?

Journal:	*Physical Chemistry Chemical Physics*
Manuscript ID	CP-ART-09-2022-004406.R1
Article Type:	Paper
Date Submitted by the Author:	26-Oct-2022
Complete List of Authors:	Southern, Scott; Ames National Laboratory, Division of Chemical and Biological Sciences Liu, Da-Jiang; Iowa State University, Ames Laboratory Chatterjee, Puranjan; Ames Laboratory; Iowa State University, Chemsitry Li, Yuting; Ames National Laboratory, Division of Chemical and Biological Sciences Perras, Frédéric A.; Ames National Laboratory, Division of Chemical and Biological Sciences

^{1}H Chemical Shift Anisotropy: A High Sensitivity Solid-State NMR Dynamics Probe for Surface Studies?

Scott A. Southern,[1] Da-Jiang Liu,[1] Puranjan Chatterjee,[1,2] Yuting Li,[1] Frédéric A. Perras[1]*

[1]Division of Chemical and Biological Sciences, Ames National Laboratory, Ames, IA 50014, USA
[2]Department of Chemistry, Iowa State University, Ames, IA 50014, USA

*Corresponding author: fperras@ameslab.gov

Abstract

Dynamics play significant roles in chemistry and biochemistry—molecular motions impact both large- and small-scale chemical reactions in addition to biochemical processes. In many systems, including heterogeneous catalysts, the characterization of dynamics remains a challenge. The most common approaches involve the solid-state NMR measurement of anisotropic interactions, in particular ^{2}H quadrupolar coupling and ^{1}H-X dipolar coupling, which generally require isotope enrichment. Due to the high sensitivity of ^{1}H NMR, ^{1}H chemical shift anisotropy (CSA) is a particularly enticing, and underexplored, dynamics probe. We carried out ^{1}H CSA and ^{1}H-^{13}C dipolar coupling measurements in a series of model supported complexes to understand how ^{1}H CSA can be leveraged to gain dynamic information for heterogeneous catalysts. Mathematical descriptions are given for the dynamic averaging of the CSA tensor, and its dependence on orientation and asymmetry. The variability of the orientation of the tensor in the molecular frame, in addition to its magnitude and asymmetry, negatively impacts attempts to extract quantitative dynamic information. Nevertheless, ^{1}H CSA measurements can reveal useful qualitative insights into the motions of a particularly dilute site, such as from a surface species.

Keywords

Molecular Dynamics, Heterogeneous Catalysis, ^{1}H Chemical Shift Anisotropy, Symmetry-Based Recoupling

1. Introduction

Dynamics are of central importance in many chemistry fields. In catalysis, they have been recognized as one of the most critical and poorly understood phenomena that could have outsized impacts on reaction outcomes.[1] For instance, structural variability in catalysts is responsible for site activation and deactivation. Dynamics that occur at equilibrium, i.e., conformational molecular dynamics, are also known to produce highly catalytically active transient species[2–4] or endow a catalyst with the ability to adapt its structure to lower reaction barriers.[5–7] This second point is perhaps best exemplified by the enzymatic concepts of allostery and induced fit.[8]

Despite the importance of understanding motions in heterogeneous catalysts, one would argue that there is a severe lack of methods available for measuring motions in highly dilute interfacial species, particularly fast motions. In the case of single-site catalysts, solid-state NMR has shown some promise for revealing the equilibrium motions of supported metal complexes but has not drawn widespread adoption.[9–12] This is primarily due to the low sensitivity of the specialized, and often multidimensional, NMR methods required for the measurement of motionally-sensitive anisotropic interactions.

The gold standard for measuring molecular motions using solid-state NMR is ^{2}H lineshape analysis.[13,14] In this experiment, the ^{2}H quadrupolar coupling tensor is measured, often as a function of temperature. If motions occur at a similar or faster rate than the magnitude of the interaction, then the NMR spectrum will reflect the average of the second rank quadrupolar coupling tensor over this timescale. Because the tensor is directional (along the X-H bond in this case), the resulting magnitude and asymmetry of the interaction are highly characteristic of the path followed by the atoms.[15]

The ^{1}H-X dipolar coupling tensor shares many of the properties that make the ^{2}H quadrupolar coupling tensor so attractive for the measurement of dynamics. Specifically, it is oriented along the X-H bond, has a predictable magnitude and asymmetry, and can be used to probe motions at multiple locations in the same molecule. It is even favored in some systems because spectral overlap may be circumvented through X-detection in a 2D acquisition, and because ^{2}H labeling is often difficult.

While they are formidable dynamics probes, ^{2}H NMR and 2D ^{1}H-X dipolar coupling measurements often require isotope enrichment when applied to supported molecules.[16–20] As such, having a viable sensitive alternative could enable the broader study of motions on heterogeneous catalyst surfaces. Both the ^{2}H quadrupolar coupling tensor and the ^{1}H-X dipolar coupling tensor probe the same property, namely, the variability in the X-H vector. There is another anisotropic interaction that affects hydrogen nuclei that may share these useful properties, while avoiding their sensitivity limitations, namely, the ^{1}H chemical shift anisotropy (CSA).[21–34] Perceived challenges with its application include the fact that it is the weakest of the three interactions, and that its more complex dependence on structure may make it difficult to predict its magnitude and orientation.

This work reviews the theory describing the dynamic averaging of the chemical shift tensor and how various dynamic modes affect its magnitude. We then compare symmetry-based ^{1}H CSA and ^{1}H-^{13}C dipolar coupling measurements for probing motions in a periodic mesoporous

organosilica (PMO) and two supported metal complexes. We highlight the challenges and limitations associated with the application of ^{1}H CSA measurements for probing dynamics in addition to its strengths.

2. Theory

2.1. Dynamic Averaging of Dipolar Coupling

Nuclear spins couple directly through a direct dipolar spin-spin coupling interaction. The interaction depends on the dipolar coupling constant (D) and the orientation of the internuclear vector, relative to the applied magnetic field. Because D depends solely on the internuclear distance, r, the vacuum magnetic permeability, μ_0, and the gyromagnetic ratios of each coupled nuclei, γ_i, (eqn. 1), it is fairly constant for bonded pairs (~23 kHz for a ^{1}H-^{13}C).

$$D_{1,2} = \left(\frac{\mu_0}{4\pi}\right)\left(\frac{\gamma_1\gamma_2}{2\pi}\right)r_{1,2}^{-3} \quad (1)$$

The spatial dependence of the interaction can be represented by a traceless and axially symmetric tensor (**D**), which in its principal axis system (PAS) takes the following form.

$$\mathbf{D}_{\mathrm{PAS}} = D\begin{bmatrix} 0.5 & 0 & 0 \\ 0 & 0.5 & 0 \\ 0 & 0 & -1 \end{bmatrix} \quad (2)$$

In this frame, the internuclear vector is oriented along the z direction. To calculate the tensor in some arbitrary, lab-frame, orientation, it is rotated using rotation matrices (**R**), shown below using the more common ZYZ convention, where α, β, and γ are Euler angles.

$$\mathbf{D}_{\mathrm{LAB}} = \mathbf{R}_{\mathrm{Z}}^{-1}(\gamma)\mathbf{R}_{\mathrm{Y}}^{-1}(\beta)\mathbf{R}_{\mathrm{Z}}^{-1}(\alpha)\mathbf{D}_{\mathrm{PAS}}\mathbf{R}_{\mathrm{Z}}(\alpha)\mathbf{R}_{\mathrm{Y}}(\beta)\mathbf{R}_{\mathrm{Z}}(\gamma) \quad (3)$$

In the fast-motion limit, i.e., when the motions of the molecule occur at a frequency exceeding the magnitude of the interaction (D), the observed dipolar coupling tensor is simply its time-average (eqn. 4). For bonded pairs, we can assume that D is constant and that only α, β, and γ are varied by the molecular motions. Note that angled brackets are used throughout to signify that this property corresponds to a dynamic average.

$$\langle\mathbf{D}\rangle = \frac{1}{t}\int_0^t \mathbf{D}_{\mathrm{LAB}}\mathrm{d}t \quad (4)$$

If a N-site jump model is used, as opposed to a time trace, then the averaged dipolar coupling tensor is given by:

$$\langle\mathbf{D}\rangle = \frac{1}{N}\sum_{\mathrm{i}=1}^{\boldsymbol{N}}\mathbf{D}_{\mathrm{LAB,\,i}} \quad (5)$$

The obtained dynamically averaged tensor, $\langle\mathbf{D}\rangle$ can then be diagonalized to extract its eigenvalues ($\langle D_{11}\rangle$, $\langle D_{22}\rangle$, $\langle D_{33}\rangle$), which are ordered as: $|\langle D_{33}\rangle| \geq |\langle D_{22}\rangle| \geq |\langle D_{11}\rangle|$. The observed averaged dipolar coupling constant, $\langle D\rangle$, is then equal to $\langle D_{33}\rangle$, and the tensor potentially loses its axial symmetry, gaining a dipolar asymmetry parameter, $\langle\eta_{\mathrm{D}}\rangle$, given by: ($\langle D_{11}\rangle$ - $\langle D_{22}\rangle$) / $\langle D_{33}\rangle$. Note that the asymmetry parameter ranges from 0, in axially symmetric cases, to 1. The amplitude

of the motions is often characterized by a single parameter known as the order parameter $\langle S_D \rangle$, which is simply the factor by which motions reduce the magnitude of the interaction.

$$\langle S_D \rangle = \frac{\langle D \rangle}{D} \quad (6)$$

In cases of continuous rotation about an axis tilted at an angle of θ relative to the bond axis, $\langle S_D \rangle$ is simply given by $\langle S_D \rangle = |(3\cos^2\theta - 1)/2|$.[15] For instance, methyl groups ($\theta = 109.4°$) generally feature ^{13}C-^{1}H dipolar couplings with $\langle S_D \rangle = 1/3$. The first-order quadrupolar interaction of a ^{2}H nucleus is averaged in exactly the same way.

2.2. Dynamic Averaging of Chemical Shift Anisotropy

Unlike the dipolar coupling tensor, the chemical shift tensor (**CS**) is neither traceless nor axially symmetric. It can be decomposed as follows.

$$\mathbf{CS}_{PAS} = \delta_{iso} + \frac{\delta_{aniso}}{2}\begin{bmatrix} -1-\eta_{CS} & 0 & 0 \\ 0 & -1+\eta_{CS} & 0 \\ 0 & 0 & 2 \end{bmatrix} \quad (7)$$

In eqn. 7 δ_{iso} corresponds to the isotropic chemical shift, δ_{aniso} is the reduced anisotropy, and η_{CS} is the asymmetry parameter of the tensor, which takes the same form as η_D. Because δ_{iso} is invariant in the presence of conformational dynamics, we can remove it from the tensor and only work with the anisotropic part, $\mathbf{CS}_{aniso}$.

$$\mathbf{CS}_{aniso} = \mathbf{CS} - \delta_{iso} \quad (8)$$

Note that the tensor components are ordered using the Haeberlen convention, i.e. as $|\delta_{ZZ} - \delta_{iso}| \geq |\delta_{XX} - \delta_{iso}| \geq |\delta_{YY} - \delta_{iso}|$. Like the dipolar coupling tensor, we can rotate this tensor to represent it in an arbitrary orientation:

$$\mathbf{CS}_{aniso,PAS} = \mathbf{R}_Z^{-1}(\gamma)\mathbf{R}_Y^{-1}(\beta)\mathbf{R}_Z^{-1}(\alpha)\mathbf{CS}_{aniso,PAS}\mathbf{R}_Z(\alpha)\mathbf{R}_Y(\beta)\mathbf{R}_Z(\gamma) \quad (9)$$

and calculate a dynamically averaged CS tensor.

$$\langle \mathbf{CS} \rangle = \delta_{iso} + \frac{1}{t}\int_0^t \mathbf{CS}_{aniso,LAB}\mathrm{d}t \quad (10)$$

We can then define a CSA order parameter by again diagonalizing $\langle \mathbf{CS} \rangle$ and calculating its resulting $\langle \delta_{aniso} \rangle$ value as: $\langle \delta_{aniso} \rangle = \langle \delta_{ZZ} \rangle - \delta_{iso}$.

$$\langle S_{CSA} \rangle = \frac{\langle \delta_{aniso} \rangle}{\delta_{aniso}} \quad (11)$$

While the mathematical treatment of the two interactions is nearly identical, extracting dynamic information from the CSA is far more challenging in practice. Because the **CS** is rarely axially symmetric, the asymmetry parameter, η_{CS} affects $\langle S_{CSA} \rangle$ to a great extent.[28] In addition, while the largest component of the dipolar coupling tensor is aligned along the internuclear axis, the chemical shift tensor originates from the local electronic environment and may take any orientation. For X-H bonded ^{1}H nuclei, it may also be more common for δ_{ZZ} to be oriented perpendicular to the bond, particularly for aryl protons. This bond is likely the dominant shielding

contributor, and it generates paramagnetic shielding contributions perpendicular to its σ-bond direction.[35,36] As such, in the very same system, $\langle S_{CSA} \rangle$ is expected to be very different from $\langle S_D \rangle$ because they probe the exchange of orthogonal axes.

In this work, we will focus on the dynamic averaging of aryl ^{1}H CSAs given that they are generally larger than the CSA found in sp^3 hybridized C-H protons[25,28] and that the small magnitude of a C-H ^{1}H site's CSA is one of the main bottlenecks that limit the measurement of $\langle S_{CSA} \rangle$. We have plotted in Figure 1 how $\langle S_{CSA} \rangle$ and the averaged CSA asymmetry parameter, $\langle \eta_{CS} \rangle$, are impacted by the main two classes of motions affecting aryl protons, namely a 2-fold flip and a plane rotation. The values are plotted as a function of the static CS asymmetry, η_{CS}, and the tensor's orientation. Note that if δ_{ZZ} is oriented perpendicular to the plane of the ring, it will be unaffected by the dynamics, i.e. $\langle S_{CSA} \rangle = 1$. As such, these sets of orientations were omitted from the Figure.

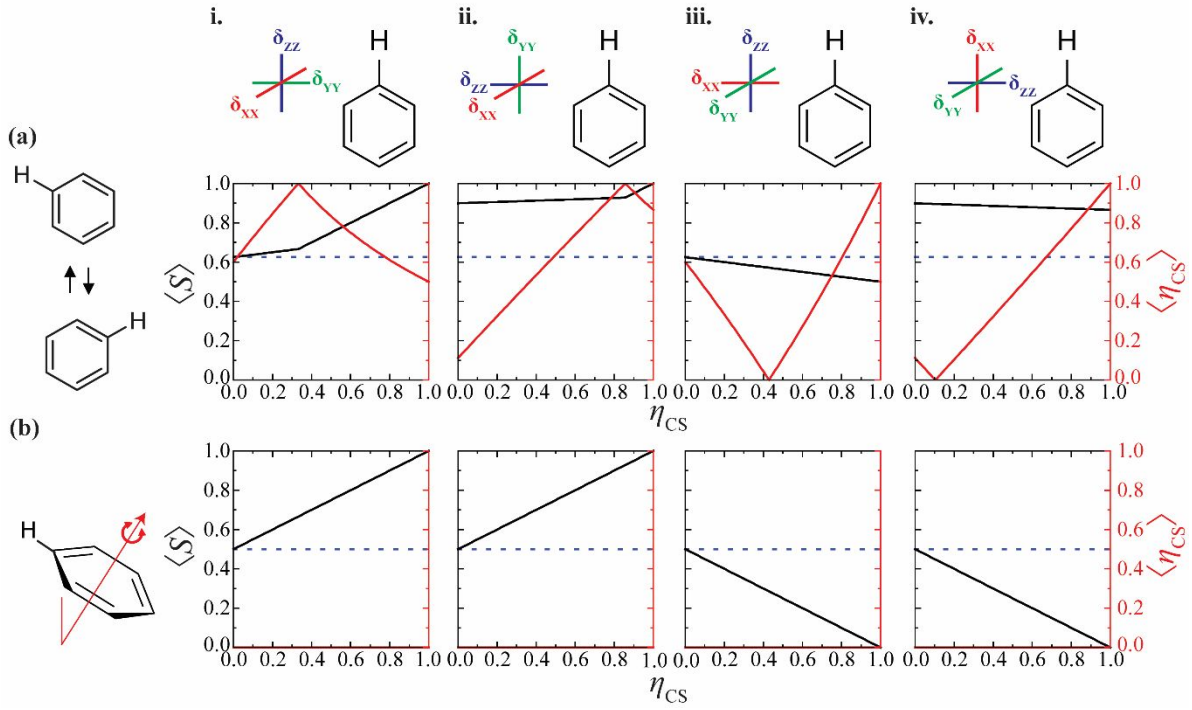

Figure 1. The dependence of $\langle S_{CSA} \rangle$ and $\langle \eta_{CS} \rangle$ on the value of η_{CS} is shown for four CS tensor orientations (i-iv), as shown on the top, for both a two-site hop model (a) as well as a continuous rotation (b). The dashed lines correspond to the behavior you would expect for ^{13}C-^{1}H dipolar coupling.

As can be seen, the magnitude of η_{CS} has a dramatic impact on the value of $\langle S_{CSA} \rangle$. For instance, if $\eta_{CS} = 1$ and δ_{XX} is oriented along the axis of rotation, the CSA is expected to be no longer sensitive to motion. Thus, for non-zero values of η_{CS}, the sensitivity of CSA to dynamics is expected to vary. It then becomes particularly difficult to extract dynamic information using the ^{1}H CSA. Given the insensitivity of *R*-type symmetry-based CSA recoupling sequences to the value

of η_{CS}, the orientation of the tensor and its asymmetry in the static limit need to be known *a priori* to evaluate $\langle S_{CSA} \rangle$. In certain cases, it may be possible to determine the static magnitude and asymmetry of the tensor by performing low-temperature measurements, but the orientation of the tensor can only be obtained experimentally using single crystal NMR.[37,38] Instead, we will apply density functional theory (DFT) calculations to estimate both the tensor's static magnitude and orientation. Note that these challenges are unique to the chemical shift tensor.

3. Experimental Methods

3.1. Synthetic Details

Ph-PMO

In a 50 mL glass vial, 1.0 g of Brij-76 was mixed with 25 mL HCl (2 M) and 5 mL nanopure water. The mixture was heated to 50 °C and stirred at 550 rpm for 0.5 h after which 5.2 mmol (2.1 mL) of 1,4-*bis* (triethoxysilyl)benzene was added. The solution was stirred for 2 h at 50 °C and then heated in an oven at 105 °C for 24 h. The resulting material was washed thoroughly with nanopure H_2O and methanol and dried overnight under vacuum. The templating agent was removed by extraction using a 0.12 M HCl solution in ethanol (150 mL) for 16 h at 50 °C, following which, the Ph-PMO was washed using ethanol and H_2O, and dried under vacuum. N_2 physisorption and powder X-ray diffraction revealed the successful formation of the PMO material (BET surface area = 1030 m^2/g, pore volume = 1.02 cm^3/g, pore diameter = 3.5 nm).

$ZnPhen/SiO_2$

The synthesis of the supported Zn phenanthroline complex was described elsewhere.[39]

Cp_2ZrOMe/SiO_2

Using an Ar glovebox, $Cp_2Zr(CH_3)_2$ (0.25 mmol, Strem) was dissolved in benzene (10 mL) and stirred with Davisil 635 silica (200 mg, Aldrich) that had been thermally treated under vacuum at 550 °C for 16 hours. The mixture was stirred overnight at room temperature. The solution was then decanted, and the resulting material was washed three times with benzene (10 mL) and dried *in vacuo* for 12 hours. ICP-MS analysis indicated a Zr weight percent of 3.85±0.1%. The obtained Cp_2ZrMe/SiO_2 species is then converted to a Cp_2ZrOMe/SiO_2 species by exposure to oxygen.[39–41]

3.2. Solid-State NMR Spectroscopy

Unless otherwise noted, all experiments were carried out on a Bruker Avance NEO 600 MHz solid-state NMR spectrometer. $^{13}C\{^1H\}$ windowed proton-detected local field (wPDLF)[42–44] experiments were carried out using a Bruker 4 mm triple resonance MAS probe operating in double resonance mode and a spinning frequency of 11.111 kHz. The w$R18^5_2$ recoupling sequence[45] was applied to the ^1H nuclei with a 50% window duration and 100 kHz radiofrequency (RF) power. Cross polarization (CP) to ^{13}C was carried out using a tangent pulse with a contact time lasting 150 us to avoid long-range polarization transfer beyond single C-H bonds. The recycle delay was set for each sample to $1.3T_1(^1H)$ to maximize the sensitivity of the experiment[46], and ranged from 1 to 5 s.

^{1}H-detected CSA recoupling measurements were carried out using a JEOL 0.75 mm fast-MAS probe using a spinning frequency of 75 kHz. The $R20\ {}^{8}_{9}\ (270_{0}90_{180})$ sequence was applied to reintroduce the ^{1}H CSA, and the signal was detected using a spin echo. The effects caused by the simultaneous recoupling of heteronuclear dipolar interactions[24,47,48] were minimized by the use of natural abundance samples. The RF power of all pulses was set to 166.67 kHz. The spectra were acquired in 16 scans per increment and 32 t_1 increments of 120 μs. The spin-lattice relaxation time was determined for each sample and the recycle delay was set to $1.3T_1(^{1}\mathrm{H})$.[46] Spectra were simulated using SIMPSON.[49]

A $^{13}\mathrm{C}\{^{1}\mathrm{H}\}$ windowed phase-alternating R-symmetry (wPARS)[44,47] experiment was carried out for the Cp_2ZrOMe/SiO_2 complex at 100 K using dynamic nuclear polarization (DNP) for sensitivity enhancement.[50–52] The sample was impregnated with a 16 mM solution of the TEKPOL[53] polarizing agent in deuterated 1,1,2,2-tetrachloroethane (TCE-d2) and inserted into the pre-cooled 3.2 mm MAS probe of the Bruker Avance III 400 MHz MAS-DNP NMR spectrometer. The wPARS experiment was carried out using the same experimental parameters as the wPDLF experiments, but the CP contact time was increased to 1.5 ms.

The random uncertainty for any peak positions (σ) is proportional to the line width (LW) of the peak and inversely proportional to the signal-to-noise ratio (SNR).[54] An approximate measurement of the uncertainty for both the dipolar and CSA splittings can be obtained using eqn. 12.[55]

$$\sigma = \sqrt{2} * \frac{\mathrm{LW}}{2(\mathrm{SNR})} \tag{12}$$

In addition to the peak position uncertainty, RF inhomogeneity can lead to additional uncertainties in the recoupled splittings. SIMPSON simulations were carried out to estimate these uncertainties. RF inhomogeneity leads to a slight widening of the CSA splittings, as well as the growth of the zero-frequency spike. From these simulations, we estimate the RF inhomogeneity in the experiments to be below 10%. Simulations with RF powers of ±10% were used to calculate an additional error term caused by RF inhomogeneity, which was added to that relating to the SNR.

3.3. Computational Chemistry

Calculations of Magnetic Shielding Tensors

DFT calculations were used to predict the static CS tensors, and their orientations. Calculations were both carried out with cluster models, using the Amsterdam density functional (ADF) program, ver. 2021.106[56], as well as using periodic boundary conditions with the CASTEP program (Materials Studio version 2018).

Cluster models built from the molecular complexes bonded to a single $OSi(OH)_3$ site, to approximate grafting, were geometry optimized at the PBE0/TZ2P level of theory[57–59]. Relativistic effects were included using the scalar zeroth-order regular approximation (ZORA).[60–63] Magnetic shielding tensors were calculated using the CPL module.[64–67]

The optimized cluster models were then grafted to an amorphous silica surface model generated by Comas-Vives.[68] Gauge-including projector-augmented-wave (GIPAW) DFT

calculations were performed on these models using CASTEP.[69–72] Geometry optimizations were carried out using the minimization approach of Broyden, Fletcher, Goldfarb, and Shanno (BFGS)[73] with fixed unit cell dimensions. The PBE functional[74] was applied with on-the-fly generated ultrasoft pseudopotentials and the scalar ZORA relativistic correction. Calculations were carried out with kinetic energy cutoffs exceeding 500 eV and 1x1x1 *k*-point grids.[75] Dispersion corrections were included using the approach of Grimme, as implemented in CASTEP.[76,77] All calculated magnetic shielding tensors were extracted from the output files using EFGShield (version 4.7.1).[78]

Molecular Dynamics Simulations

We performed machine learning (ML)-accelerated molecular dynamics (MD) simulations using the DeePMD framework.[79] For the Zr metallocene complex, a total of 200 individual MD simulations (each one around 2000 time steps) were performed using VASP[80–83] and used to train a DeePMD potential (`se_e2_a`) descriptor. DFT calculations were performed using the PBE functional, 400 eV energy cutoff for basis sets, Γ point only *k*-point grid, and 0.2 eV Gaussian smearing of the electron occupancy. More details of the methodology can be found in ref [84].

4. Results and Discussion

The following sections will cover the NMR studies of the dynamics of three species using both ^{1}H CSA and ^{1}H-^{13}C dipolar coupling measurements. The first sample is a phenyl (Ph)-PMO[85,86] (section 4.1) for which the phenyl moieties have been shown to behave as molecular rotors using NMR spectroscopy.[87,88] It serves as a control to demonstrate the sensitivity of the methods to molecular motions of aryl functionalities. The second sample is a silica-tethered Zn phenanthroline complex (section 4.2). Its structure was recently solved to a high level of precision using NMR-based distance measurements[39] and suggests secondary complex-support interactions that might hinder dynamics. The last sample is a monopodal grafted Zr metallocene complex (section 4.3) for which two dynamic modes are expected, namely cyclopentadienyl (Cp) rotation, and a Si-O and/or O-Zr rotation. Due to its low metal loading, conventional NMR and ^{1}H-^{13}C dipolar coupling measurements are particularly challenging, and it is used to probe whether ^{1}H CSA can be used to gain unique insights into its dynamics and local environment.

Experimentally-determined dipolar coupling and chemical shift tensor parameters are given in Tables 1 and 2, respectively. DFT-calculated ^{1}H CS tensor parameters are given in Table 3.

Table 1. ^{13}C{^{1}H} dipolar order parameters

Sample	Site	δ_{iso} / ppm	$\langle S_D \rangle$
Ph-PMO	Ph	131.7 ± 0.02	0.56 ± 0.19
ZnPhen/SiO_2	C_I	146.7 ± 0.4	1.01 ± 0.13
	C_G	136.3 ± 0.7	1.00 ± 0.12
	C_D	123.4 ± 0.2	1.02 ± 0.25
	C_C	40.5 ± 0.1	0.95 ± 0.27
	C_B	21.9 ± 0.07	0.25 ± 0.17
	C_A	7.3 ± 0.1	0.85 ± 0.24

$Cp2ZrOMe/SiO_2$[a]	Cp	113.9 ± 0.02	0.52 ± 0.18

[a]Measurement was performed at 100 K.

Table 2. Experimental ^{1}H CS tensor parameters

Sample	δ_{iso} / ppm	$\langle S_{CSA} \rangle$	$\langle \delta_{aniso} \rangle$ / ppm
Ph-PMO	6.95 ± 0.01	1.0	8.5 ± 0.3
$ZnPhen/SiO_2$	7.28-8.3 ± 0.09	0.8-1.0	5.5-6.9 ± 0.4
	0.10-1.81 ± 0.09	0.7	4.6 ± 0.5
Cp_2ZrOMe/SiO_2	5.64 ± 0.01	1.0	5.2 ± 0.4

Table 3. DFT-calculated ^{1}H CS tensor parameters

		Orientations[a]		*Cluster models*		*Periodic models*	
Sample	Site	⊥ to ring	|| to C-H	$\lvert\delta_{aniso}\rvert$ / ppm	η_{CS}	$\lvert\delta_{aniso}\rvert$ / ppm	η_{CS}
Ph-PMO		σ_{YY}	σ_{ZZ}	7.9-13.1	0.5-1.0	12.1-13.2	0.33-0.36
$ZnPhen/SiO_2$	I	σ_{ZZ} / σ_{XX}	σ_{XX} / σ_{YY}	5.1	0.9	4.4	0.9
	G	σ_{ZZ}	σ_{YY}	5.9	0.8	3.6	0.7
	D	σ_{ZZ}	σ_{XX} / σ_{YY}	5.6	0.2	2.5	0.4
	D’	σ_{ZZ}	σ_{YY}	8.8	0.8	5.8	0.8
Cp_2ZrOMe/SiO_2		σ_{XX} / σ_{YY}	σ_{ZZ}	1.4-2.5	0.1-0.9	1.7-4.9	0.49-0.97

[a]Tensor orientations were not found to be model-dependent.

4.1. Ph-PMO

The Ph moieties in the Ph-PMO material are expected to rotate and perform 2-fold jumps, as described in Figure 2, top. These motions are expected to yield a ^{1}H-^{13}C $\langle S_D \rangle$ value of 0.625 and increase the observed dipolar asymmetry parameter to 0.6. The ^{13}C{^{1}H} wPDLF spectrum acquired on this sample (Figure 2a) reveals a 4.4 ± 0.07 kHz splitting, equating to a 13 kHz $\langle D \rangle$ value and $\langle S_D \rangle$ = 0.56. The value agrees with a previous ^{2}H NMR study that observed the same two-fold jumps.[88] The 10% lower $\langle S_D \rangle$ value may be caused by a combined rotation/libration.

The CSA-recoupled ^{1}H spectrum is shown in Figure 2b. The aromatic resonance from the Ph groups (6.95 ppm) produces a 1.0 ± 0.01 kHz CSA splitting, as depicted in Figure 2c. A SIMPSON simulation was carried out to determine $\langle \delta_{aniso} \rangle$ and $\langle \eta_{CS} \rangle$. The best fit (Figure 2c, red line) was obtained with $\langle \delta_{aniso} \rangle$ = 8.5 ppm and $\langle \eta_{CS} \rangle$ = 0.6. These values are in the same range as those measured by Damron *et al.* where aromatic protons in acetaminophen exhibit ^{1}H anisotropies of 5-7.5 ppm.[89]

Both cluster-based and periodic DFT calculations were performed to estimate the static ^{1}H CSA magnitude and tensor orientation. A cluster model was built by repeating the basic unit 5 times to form a stacked chain (Figure 3b). The value δ_{aniso} was found to be extremely sensitive to the atom’s position relative to the neighboring aromatic rings. For instance, ^{1}H nuclei in the central aromatic ring experience a shielding anisotropy of 13 ppm (η_{CS} = 0.5) while the flanking rings had

predicted ^{1}H δ_{aniso} values of approximately 12 ppm (η_{CS} = 0.5-0.6), and the rings on the extremities had ^{1}H δ_{aniso} values of 8-8.5 ppm (η_{CS} = 0.9-1,

Table 3). In the periodic model, all ^{1}H nuclei experience the larger anisotropy as they are effectively all internal moieties. As it is impossible to know whether our models are truly accurate, this surprising variability hampers our ability to extract chemical shift order parameters from the sample. Similar variations in ^{1}H CSAs have also been observed in hydrogen-bonded systems.[90] The calculations do, however, clearly predict that the δ_{ZZ} tensor component is oriented along the C-H internuclear vector and should be sensitive to dynamics. The component oriented perpendicular to the ring is expected to be δ_{YY}.

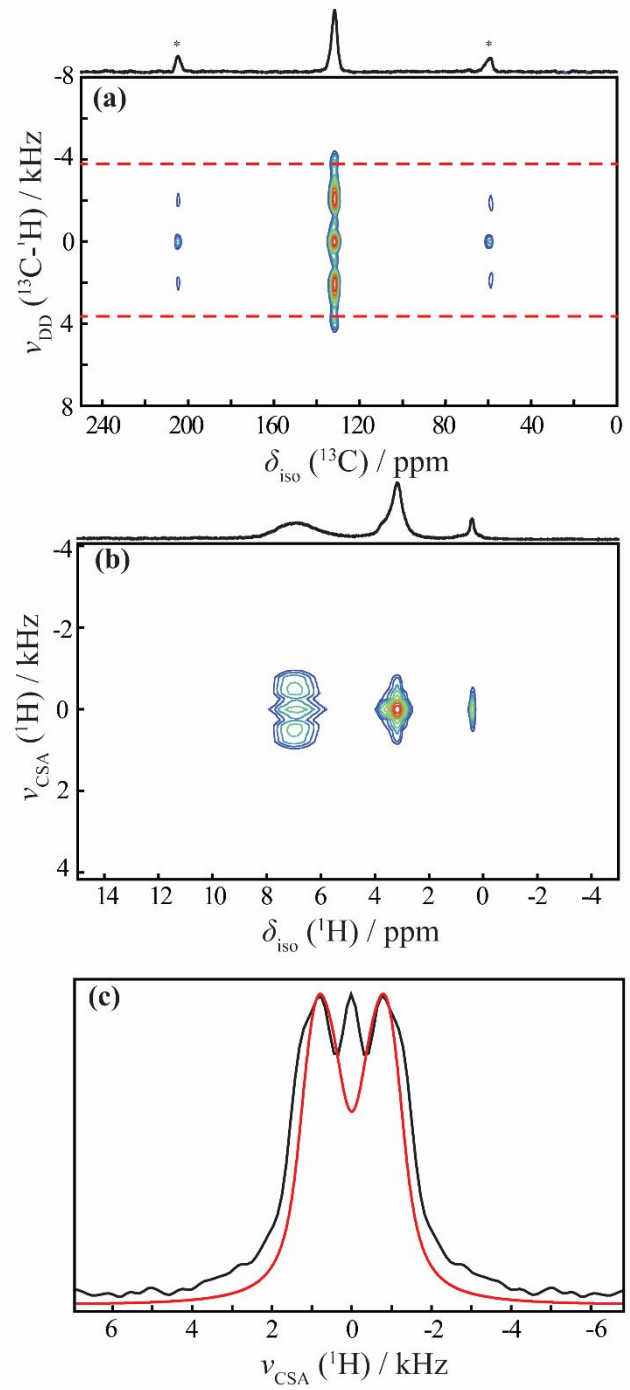

Figure 2. ^{13}C{^{1}H} wPDLF (a) $R20_{9}^{8}$ ($270_{0}90_{180}$)-based ^{1}H CSA-recoupled (b) spectra measured on a Ph-PMO. The red dashed lines in (a) indicate the approximate splitting expected for an immobile C-H spin pair. The CSA-recoupled lineshape for the aromatic ^{1}H signal is shown in (c) with a fit in red.

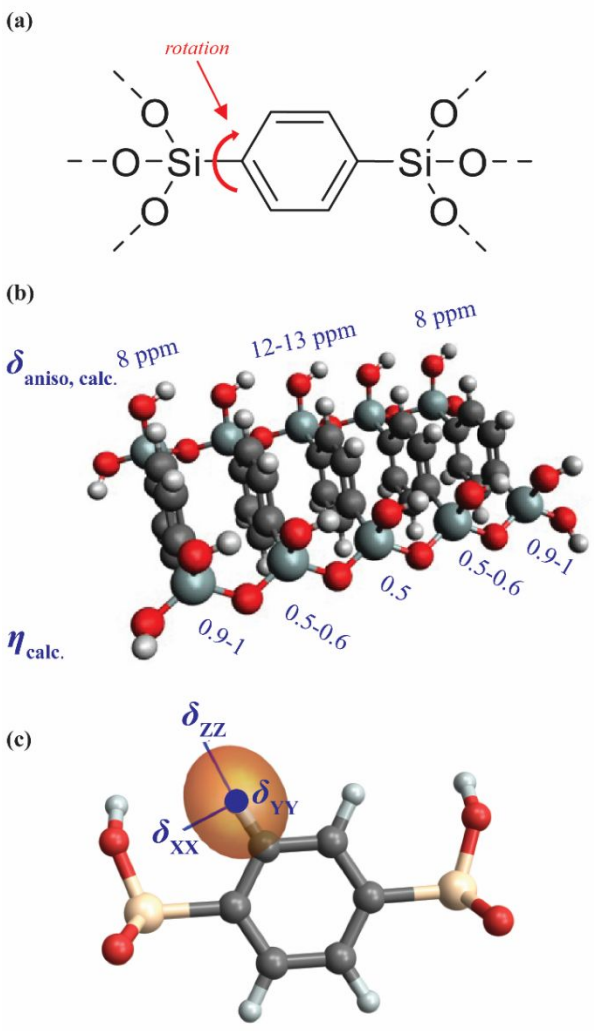

Figure 3. (a) Chemical structure of the basic building unit of the Ph-PMO. (b) Cluster representation of a Ph-PMO chain showing the calculated range of aromatic ^{1}H δ_{aniso} and η_{CS} values. (c) Representation of the CS tensor orientation for a selected phenyl-hydrogen calculated using GIPAW DFT (see Table 3).

Looking at the data in Figure 1aiii, the experimentally-observed anisotropy, $\langle\eta_{CS}\rangle$, of 0.6 could originate from two tensors, namely those with: 1) $\langle S_{CSA}\rangle$ = 0.625, δ_{aniso} = 13.6 ppm, η_{CS} = 0.0, or 2) $\langle S_{CSA}\rangle$ = 0.526, δ_{aniso} = 16.2 ppm, η_{CS} = 0.79. The second δ_{aniso} value is far too large and as such the first option is likely correct. It is also possible that the DFT calculations incorrectly predicted the tensor orientations and that δ_{XX} could be perpendicular to the ring with $\langle S_{CSA}\rangle$ = 0.905, δ_{aniso} = 9.4 ppm, η_{CS} = 0.81. Both options agree with the tensor magnitudes and asymmetry parameters from either the plane-wave or cluster model DFT calculations and thus also corroborate the dipolar coupling measurement suggesting the presence of 2-fold ring flips. While this shows that dynamic information is available from ^{1}H CSA measurements, it does depend on our ability to determine $\langle\eta_{CS}\rangle$[25] and even then, leads to many competing interpretations. The DFT calculations

were also sufficiently ambiguous that one might have assumed a non-dynamic $\delta_{aniso} = 8.5$ ppm site instead of the dynamic one.

4.2. ZnPhen/SiO_2

A $^{13}C\{^1H\}$ wPDLF experiment was performed on ZnPhen/SiO_2 at room temperature to assess whether the complex releases from the surface at 300 K. As mentioned earlier, NMR-based distance measurements performed on this complex have shown evidence for the formation of secondary complex-support interactions at low temperatures.[39] If such interactions are indeed present, we would expect the complex to remain bound to the support and have only limited motions, unlike other grafted organic species that have been studied using NMR.[18,20] The wPDLF measurement resulted in recoupled dipolar splittings of 7.8 ± 0.2 to 8.0 ± 0.09 kHz for the aromatic sites, slightly higher than the expected value of 7.8 ± 0.4 kHz in the case of a non-dynamic CH spin pair[12] corresponding to a $\langle S_D \rangle$ value of approximately 1.0 (Figure 4). As such, the phenanthroline moiety does not undergo any dynamic averaging, confirming that indeed the complex is immobilized on the silica surface. Conversely, the CH_2 pairs A, B, and C show higher degrees of motion with $\langle S_D \rangle$ values of 0.85, 0.25, and 0.95, respectively, indicating that the surface tether retains some level of conformational freedom.

While successful, the wPDLF experiment suffered from extremely low sensitivity. The spectrum required a minimum of 18 hours to acquire with sufficient signal to noise. Unlike the Ph-PMO, the ZnPhen complex is located exclusively on the external surface of the silica material. If the same information could be obtained using solely ^1H NMR it would represent a dramatic reduction in experiment time. We measured the ^1H CSA using the $R20\,^{8}_{9}\,(270_{0}90_{180})$ recoupling sequence under fast-MAS (see Figure 4c). The spectrum suffers from poor resolution in the aromatic region, which nevertheless appears to suggest the presence of a distribution of CSA parameters, likely from the overlap of the four chemically inequivalent sites.

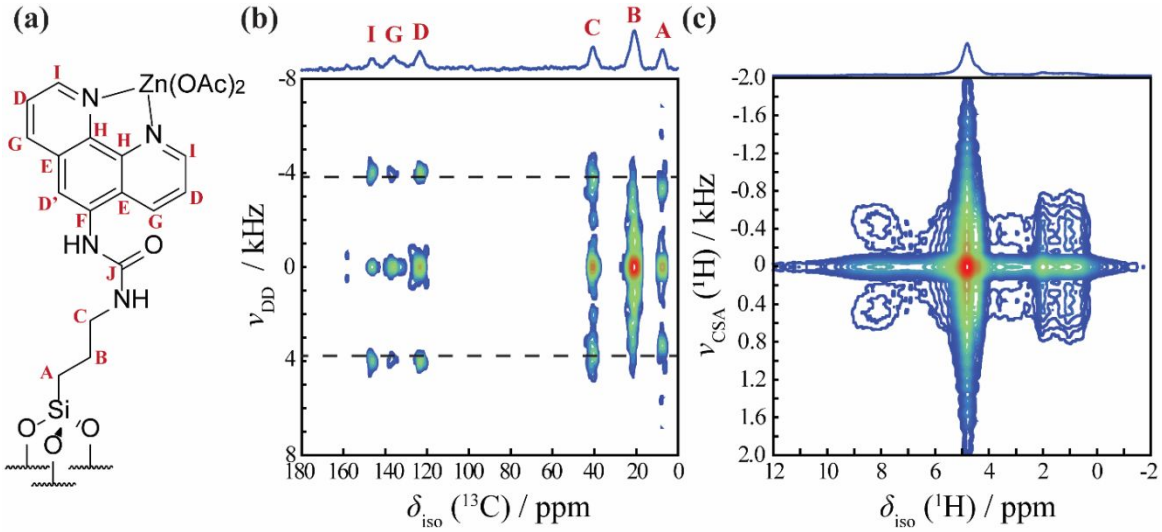

Figure 4. (a) Structure and site assignment of ZnPhen/SiO_2. (b) $^{13}C\{^1H\}$ wPDLF spectrum; red dashed lines indicate the approximate splitting expected for an immobile C-H spin pair. (c) ^1H CSA recoupling spectrum using the $R20\ {}^{8}_{9}\ (270_0 90_{180})$ sequence.

Figure 5a shows indirect dimension slices taken from the spectrum in Figure 4c at a range of chemical shifts in the aromatic spectral region. The spectra show evidence of a positive correlation between $\langle\delta_{aniso}\rangle$ and δ_{iso}. This broadening could either arise from a variability of the magnitude of δ_{aniso} and η_{CS} or a distribution of $\langle S_{CSA}\rangle$ values. For instance, all three H_D and $H_{D'}$ protons are sensitive to N-C_F rotations, but only half of H_I and H_G protons are.

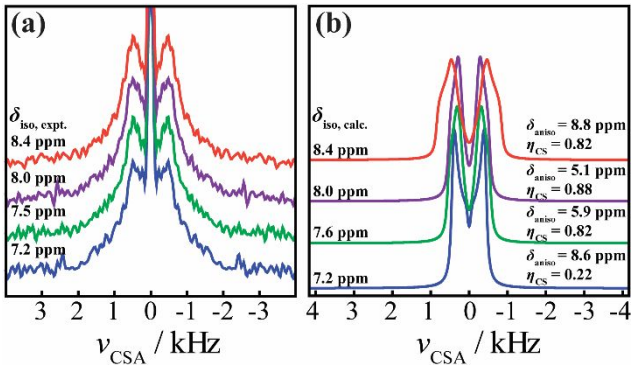

Figure 5. (a) One-dimensional, indirect dimension, slices of the ^1H CSA-recoupled spectrum of ZnPhen/SiO_2 taken at the indicated proton chemical shifts. (b) Simulated CSA-recoupled spectra for the four chemically-distinct sites, using the parameters predicted using DFT, as indicated on the Figure. Calculated chemical shifts were determined by a linear regression analysis of the relationship between $\sigma_{iso,calc.}$ and $\delta_{iso,expt.}$ over these data points to find a reference expression, namely: $\delta_{iso,calc.} = -0.4834\sigma_{iso,calc.} + 19.116$ ppm and $R^2 = 0.9665$.

DFT calculations were performed on a model cluster to predict CSA parameters of the aromatic protons. As seen in

Table 3 and Figure 5b, calculated δ_{aniso} and η_{CS} values are in the same range as those measured experimentally, and also predict a positive correlation between δ_{iso} and the recoupled CSA splitting. As such, it is likely that the measured CSA parameters are indeed the static values, and that the ZnPhen complex interacts with the support, in agreement with that determined using the dipolar coupling measurements.

4.3. Cp_2ZrOMe/SiO_2

The last complex, a Zr metallocene grafted to silica gel (Cp_2ZrOMe/SiO_2, Figure 6a), could not be studied using conventional $^{13}C\{^1H\}$ NMR spectroscopy due to sensitivity limitations. As such, we applied DNP for sensitivity enhancement.[50–52] Cp rotation is known to have a particularly low barrier[91–95] and we would thus expect to see rotational motions down to 100 K. The DNP-enhanced $^{13}C\{^1H\}$ wPARS NMR spectrum we obtained is shown in Figure 6b. Two resonances are observed at 113.9 ± 0.02 and 75 ± 0.04 ppm, which are attributed to the Cp rings and the Zr-bound methoxy group.

As can be observed by the positions of the wPARS peaks relative to the dashed red lines that indicate the static dipolar splittings in Figure 6b, the dipolar couplings for both sites are significantly reduced due to dynamics. No splitting is observed for the methoxy group, while a $\langle S_D \rangle$ value of 0.52 ± 0.03 can be obtained for the Cp carbons. As described in section 2.1, a continuous rotation of the Cp groups should lead to a $\langle S_D \rangle$ value of $|(3\cos^2(90°) - 1)/2| = 0.5$, which is in agreement with the observation.[15] Therefore, we can conclude that, at 100 K, the Cp rings are freely rotating while the rest of the complex is stationary.

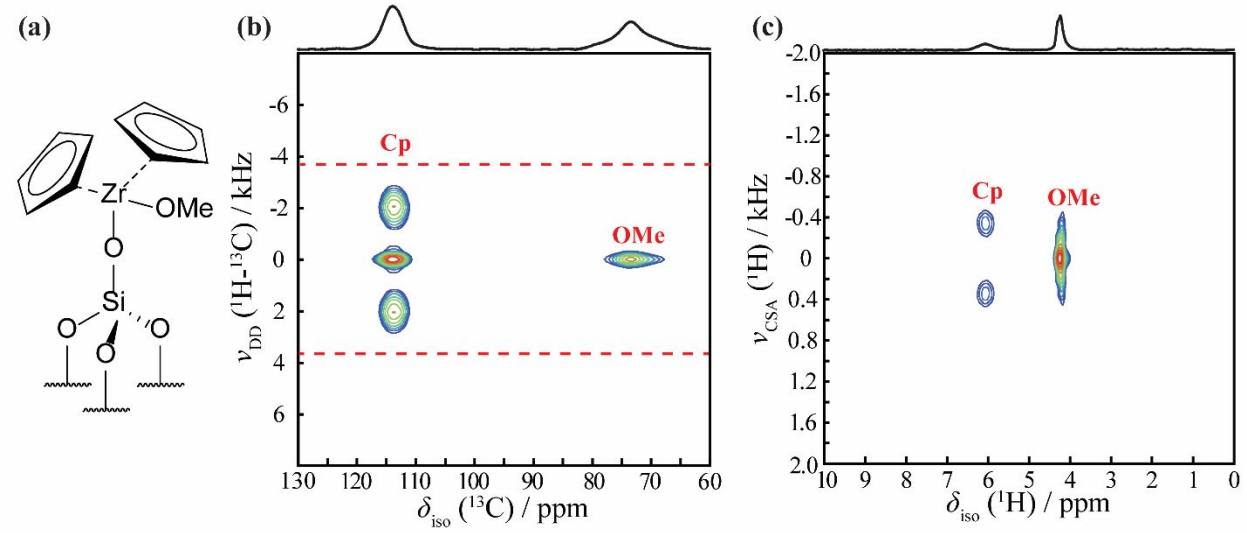

Figure 6. (a) Structure of Cp_2ZrOMe/SiO_2. (b) DNP-enhanced $^{13}C\{^1H\}$ wPARS NMR spectrum; red dashed lines indicate the expected splitting for an immobile C-H spin pair. (c) ^{1}H CSA recoupling spectrum using the $R20\,{}^{8}_{9}\,(270_0 90_{180})$ sequence.

While the DNP experiment could reveal the rotations of the Cp rings, the dynamics of the complex at room temperature remain ambiguous. A Zr-OMe resonance confirms that the complex only forms one Si-O-Zr linkage with the support and, as such, may be able to freely rotate about these bonds. This form of dynamics has been observed in some supported olefin metathesis catalysts.[10] We performed periodic MD simulations of the complex grafted to an amorphous silica model of Comas-Vives[68] (Figure 8a). The speed of the simulations was accelerated using machine learning (ML)[84] which allowed for the treatment of such a large complex and surface model. Figure 8aii (black) shows the predicted averaging of the dipolar coupling tensor; the asymptotic value corresponds to the calculated $\langle S_D \rangle$ value, namely 0.25. Figure 8aiii shows the time dependence of the surface-O-Zr-OMe dihedral angle, clearly indicating that the complex does in fact rotate about its surface tether. Note that the exchange of the Cp rings due to this rotation would lead to a composite dynamic model combining a 2-site jump (the Cp-Zr-Cp angle is close to 120°) with the continuous rotation and an $\langle S_D \rangle = 0.625 * 0.5 = 0.3125$, close to the value predicted using ML MD. The question thus remains whether the ^{1}H CSA measurements can reveal whether these motions occur in the real sample.

DFT calculations were performed to estimate the values of δ_{aniso} and η_{CS} for each of the Cp hydrogens, as well as the orientation of the tensors. Table 3 shows that the calculated values of

δ_{aniso} vary generally between 2 and 5 ppm, while η_{CS} tends to be greater than 0.5. The variability of these values is likely related to the relative proximity of each hydrogen atom to the methoxy or the silica surface while the ring is kept stationary for this calculation. The direction of δ_{ZZ} is generally predicted to be oriented along the C-H bond, with variable δ_{XX} and δ_{YY} orientations**.**

The 2D $R20\ {}^{8}_{9}\ (270_0 90_{180})$-based ^{1}H CSA recoupling spectrum is shown in Figure 6c with the projection shown in Figure 7 (bottom trace). The spectrum is best fit to a $\langle\delta_{aniso}\rangle$ value of 5.2 ppm and an axially symmetric tensor. Looking at the plots showing the dependence of $\langle S_{CSA}\rangle$ on the tensor asymmetry and orientation (Figure 1), we can see that a very low $\langle S_{CSA}\rangle$ is predicted if δ_{YY} is perpendicular to the Cp ring, while the reverse is true if δ_{XX} is perpendicular to the ring. Given that the experimentally determined $\langle\delta_{aniso}\rangle$ value is on the upper end of those predicted using DFT, we can thus only assume that δ_{XX} is predominantly oriented perpendicular to the ring and that η_{CS} is close to 1. The high value of $\langle\delta_{aniso}\rangle$ also strongly suggests that there are no Si-O-Zr rotations at room temperature, in contrast with the prediction made using ML MD. This is also well-evidenced by the CSA lineshape itself. The 2-fold jump model would see an increase in value of $\langle\eta_{CS}\rangle$ to 0.6 (Figure 1), which does not agree with the observed lineshape (Figure 7).

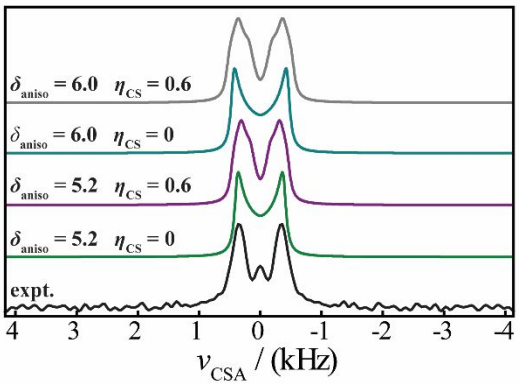

Figure 7. SIMPSON simulations comparing different values of $\langle\delta_{aniso}\rangle$ and $\langle\eta_{CS}\rangle$ on the experimental spectrum.

One potential explanation for the disagreement between the ML MD simulations and the experimental result is that the Zr concentration is quite high at 3.85 %, corresponding to a Zr surface density of 0.5 Zr/nm^2. As a result, clustering is likely to occur[96–99], leading to steric interactions that could hinder dynamics. We thus created a second model containing two Zr centers in close proximity of one another (Zr-Zr distance of 0.56 nm) and repeated the ML MD simulations. The results (Figure 8b) show that the rotation around the O-Zr bond is far more constrained. For instance, the surface-O-Zr-OMe dihedral angle (ϕ) is more constant (Figure 8bii), and the $\langle S_{CSA}\rangle$ value converges closer to 0.5 (Figure 8biii). This value is still higher than that measured experimentally; we assume that a more accurate model, containing many more Zr complexes would be able to reproduce the experimentally determined order parameters. It is also possible that surface curvature is further constraining motions.[12] A simulation was carried out on a similar model but with more numerous and equally distributed complexes (typical direct neighboring Zr-Zr distances of 0.85 to 1.36 nm), which resulted in a less restrained movement of

the complexes and a similar result to that calculated in Figure 8a. We hypothesize that average Zr-Zr distances must thus be below 0.56 nm. Alternatively, a hydrogen bonding interaction between the methoxy group and silanols may prevent the rotation of the complex, but this was not observed in the ML MD simulations.

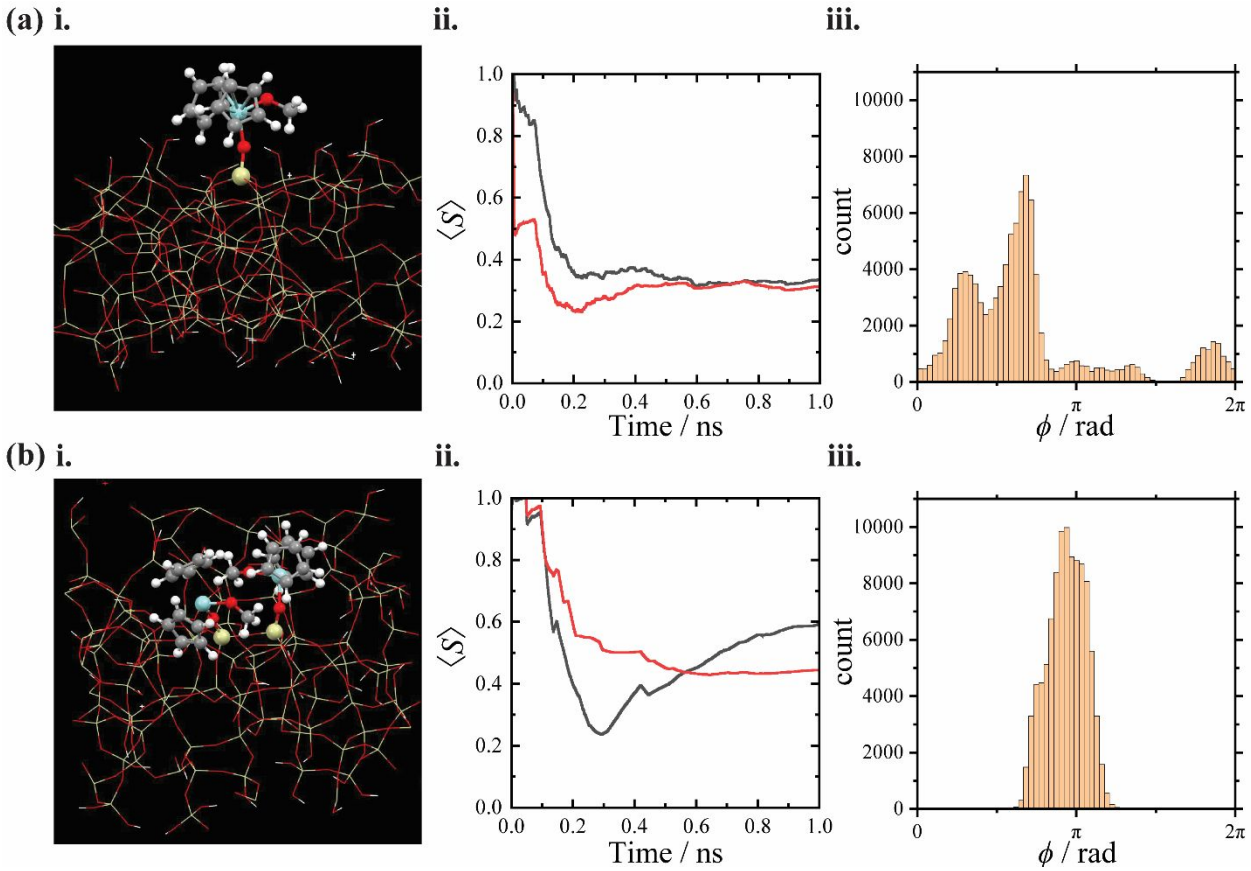

Figure 8. Results of ML MD simulations for models containing one (a) or two (b) Zr complexes. (i) Structure of the model. (ii) Plot of the surface-O-Zr-OMe dihedral angle (ϕ) as a function of simulation time. (iii) Plots showing the convergence of $\langle S_D \rangle$ (black) and $\langle S_{CSA} \rangle$ (red) as a function of simulation time. Data are analyzed using the procedure described in ref [12].

5. Conclusions

We have investigated the use of ^{1}H CSA for the measurement of dynamics, with a particular emphasis placed on the study of supported complexes. Measurements of ^{1}H-^{13}C order parameters were also performed as controls. In contrast with the measurement of ^{1}H-^{13}C dipolar coupling constants, ^{1}H CSA offers a far higher sensitivity and shorter experimental times. The CSA measurements, however, have several disadvantages that complicate their usefulness. For instance, the variability in the magnitude of δ_{aniso} and the presence of axial asymmetry can lead to greater order parameters than those measured using dipolar coupling. In addition, the sensitivity of the CSA to motions is highly dependent on the tensor orientation in the molecule frame, a factor which is often difficult to predict. Without knowing the static: 1) tensor orientation, 2) magnitude, and 3)

asymmetry, it is extremely challenging to determine any quantitative dynamic information from a ^{1}H CSA measurement. These challenges are further compounded by the insensitivity of *R*-type symmetry recoupled CSA lineshapes to tensor asymmetry, which limits our ability to determine the symmetry of the motions. Improvements to the recently reported ^{1}H ROCSA sequence[33,100] may facilitate the measurement of ^{1}H CSA asymmetry in cases where the anisotropy is weak. At this time, ^{2}H quadrupolar and ^{1}H-X dipolar coupling measurements should remain the "gold standards" for evaluating molecular dynamics using solid-state NMR, but ^{1}H CSA measurements can serve as a useful Boolean tool to determine whether a given surface site is dynamic in cases where sensitivity is limited.

Acknowledgments

This work was supported by the U.S. Department of Energy (DOE), Office of Basic Energy Sciences, Division of Chemical Sciences, Geosciences, and Biosciences through a DOE Early Career Project (SAS and FAP). Molecular dynamics calculations (DJL) were supported by the Ames National Laboratory Chemical Physics program. Ames National Laboratory is operated for the DOE by Iowa State University under Contract No. DE-AC02-07CH11358.

References

1 K. F. Kalz, R. Kraehnert, M. Dvoyashkin, R. Dittmeyer, R. Gläser, U. Krewer, K. Reuter and J. Grunwaldt, Future Challenges in Heterogeneous Catalysis: Understanding Catalysts under Dynamic Reaction Conditions, *Chemcatchem*, 2017, 9, 17–29.

2 H. Zhai and A. N. Alexandrova, Fluxionality of Catalytic Clusters: When It Matters and How to Address It, *ACS Catal*, 2017, 7, 1905–1911.

3 H. Zhai and A. N. Alexandrova, Local Fluxionality of Surface-Deposited Cluster Catalysts: The Case of Pt_7 on Al_2O_3, *J Phys Chem Lett*, 2018, 9, 1696–1702.

4 B. Zandkarimi and A. N. Alexandrova, Dynamics of Subnanometer Pt Clusters Can Break the Scaling Relationships in Catalysis, *J Phys Chem Lett*, 2019, 10, 460–467.

5 A. Kohen, Role of Dynamics in Enzyme Catalysis: Substantial versus Semantic Controversies, *Accounts Chem Res*, 2015, 48, 466–473.

6 B. R. Goldsmith, B. Peters, J. K. Johnson, B. C. Gates and S. L. Scott, Beyond Ordered Materials: Understanding Catalytic Sites on Amorphous Solids, *ACS Catal*, 2017, 7, 7543–7557.

7 O. Rivoire, Geometry and Flexibility of Optimal Catalysts in a Minimal Elastic Model, *J Phys Chem B*, 2020, 124, 807–813.

8 J. Guo and H.-X. Zhou, Protein Allostery and Conformational Dynamics, *Chem Rev*, 2016, 116, 6503–6515.

9 J. O. Ehresmann, P. W. Kletnieks, A. Liang, V. A. Bhirud, O. P. Bagatchenko, E. J. Lee, M. Klaric, B. C. Gates and J. F. Haw, Evidence from NMR and EXAFS Studies of a Dynamically Uniform Mononuclear Single-Site Zeolite-Supported Rhodium Catalyst, *Angewandte Chemie Int Ed*, 2006, 45, 574–576.

10 F. Blanc, J.-M. Basset, C. Copéret, A. Sinha, Z. J. Tonzetich, R. R. Schrock, X. Solans-Monfort, E. Clot, O. Eisenstein, A. Lesage and L. Emsley, Dynamics of Silica-Supported Catalysts Determined by Combining Solid-State NMR Spectroscopy and DFT Calculations, *J Am Chem Soc*, 2008, 130, 5886–5900.

11 D. P. Estes, C. P. Gordon, A. Fedorov, W.-C. Liao, H. Ehrhorn, C. Bittner, M. L. Zier, D. Bockfeld, K. W. Chan, O. Eisenstein, C. Raynaud, M. Tamm and C. Copéret, Molecular and Silica-Supported Molybdenum Alkyne Metathesis Catalysts: Influence of Electronics and Dynamics on Activity Revealed by Kinetics, Solid-State NMR, and Chemical Shift Analysis, *J Am Chem Soc*, 2017, 139, 17597–17607.

12 A. L. Paterson, D.-J. Liu, U. Kanbur, A. D. Sadow and F. A. Perras, Observing the three-dimensional dynamics of supported metal complexes, *Inorg Chem Front*, 2021, 8, 1416–1431.

13 P. M. J. Szell, S. Zablotny and D. L. Bryce, Halogen bonding as a supramolecular dynamics catalyst, *Nat Commun*, 2019, 10, 916.

14 B. Berglund and J. Tegenfeldt, The determination of quadrupole coupling tensors from single-crystal NMR data, *J Magnetic Reson 1969*, 1978, 30, 451–455.

15 J. J. Kinnun, A. Leftin and M. F. Brown, Solid-State NMR Spectroscopy for the Physical Chemistry Laboratory, *J Chem Educ*, 2013, 90, 123–128.

16 B. Boddenberg, R. Grosse and U. Breuninger, ^{2}H NMR spectra of trimethylsilyl groups anchored on a silica surface, *Surf Sci Lett*, 1986, 173, L655–L658.

17 T. Kobayashi, J. A. DiVerdi and G. E. Maciel, Silica Gel Surface: Molecular Dynamics of Surface Silanols, *J Phys Chem C*, 2008, 112, 4315–4326.

18 J. Gath, G. L. Hoaston, R. L. Vold, R. Berthoud, C. Copéret, M. Grellier, S. Sabo-Etienne, A. Lesage and L. Emsley, Motional heterogeneity in single-site silica-supported species revealed by deuteron NMR, *Phys Chem Chem Phys*, 2009, 11, 6962–6971.

19 Q. Wang, E. Jordan and D. F. Shantz, ^{2}H NMR Studies of Simple Organic Groups Covalently Attached to Ordered Mesoporous Silica, *J Phys Chem C*, 2009, 113, 18142–18151.

20 S. Jayanthi, V. Frydman and S. Vega, Dynamic Deuterium Magic Angle Spinning NMR of a Molecule Grafted at the Inner Surface of a Mesoporous Material, *J Phys Chem B*, 2012, 116, 10398–10405.

21 M. Hohwy, J. T. Rasmussen, P. V. Bower, H. J. Jakobsen and N. C. Nielsen, 1H Chemical Shielding Anisotropies from Polycrystalline Powders Using MSHOT-3 Based CRAMPS, *J Magn Reson*, 1998, 133, 374–378.

22 D. H. Brouwer and J. A. Ripmeester, Symmetry-based recoupling of proton chemical shift anisotropies in ultrahigh-field solid-state NMR, *J Magn Reson*, 2007, 185, 173–178.

23 L. Duma, D. Abergel, P. Tekely and G. Bodenhausen, Proton chemical shift anisotropy measurements of hydrogen-bonded functional groups by fast magic-angle spinning solid-state NMR spectroscopy, *Chem Commun*, 2008, 2361–2363.

24 G. Hou, S. Paramasivam, S. Yan, T. Polenova and A. J. Vega, Multidimensional Magic Angle Spinning NMR Spectroscopy for Site-Resolved Measurement of Proton Chemical Shift Anisotropy in Biological Solids, *J Am Chem Soc*, 2013, 135, 1358–1368.

25 H. K. Miah, D. A. Bennett, D. Iuga and J. J. Titman, Measuring proton shift tensors with ultrafast MAS NMR, *J Magn Reson*, 2013, 235, 1–5.

26 M. K. Pandey and Y. Nishiyama, Determination of NH proton chemical shift anisotropy with ^{14}N–^{1}H heteronuclear decoupling using ultrafast magic angle spinning solid-state NMR, *J Magn Reson*, 2015, 261, 133–140.

27 M. K. Pandey, M. Malon, A. Ramamoorthy and Y. Nishiyama, Composite-180° pulse-based symmetry sequences to recouple proton chemical shift anisotropy tensors under ultrafast MAS solid-state NMR spectroscopy, *J Magn Reson*, 2015, 250, 45–54.

28 R. Zhang, K. H. Mroue and A. Ramamoorthy, Proton chemical shift tensors determined by 3D ultrafast MAS double-quantum NMR spectroscopy, *J Chem Phys*, 2015, 143, 144201.

29 M. K. Pandey and Y. Nishiyama, Determination of relative orientation between ^{1}H CSA tensors from a 3D solid-state NMR experiment mediated through ^{1}H/^{1}H RFDR mixing under ultrafast MAS, *Solid State Nucl Mag*, 2015, 70, 15–20.

30 Y. Ge, I. Hung, X. Liu, M. Liu, Z. Gan and C. Li, Measurement of amide proton chemical shift anisotropy in perdeuterated proteins using CSA amplification, *J Magn Reson*, 2017, 284, 33–38.

31 H. K. Miah, R. Cresswell, D. Iuga and J. J. Titman, ^{1}H CSA parameters by ultrafast MAS NMR: Measurement and applications to structure refinement, *Solid State Nucl Mag*, 2017, 87, 67–72.

32 L. Liang, G. Hou and X. Bao, Measurement of proton chemical shift anisotropy in solid-state NMR spectroscopy, *Solid State Nucl Mag*, 2018, 93, 16–28.

33 T. Kobayashi, F. A. Perras and Y. Nishiyama, Determination of the chemical shift tensor anisotropy and asymmetry of strongly dipolar coupled protons under fast MAS, *Solid State Nucl Mag*, 2021, 114, 101743.

34 F. A. Perras, A. L. Paterson and T. Kobayashi, Phase-sensitive γ-encoded recoupling of heteronuclear dipolar interactions and ^{1}H chemical shift anisotropy, *Solid State Nucl Mag*, 2021, 111, 101712.

35 N. F. Ramsey, Magnetic Shielding of Nuclei in Molecules, *Phys Rev*, 1950, 78, 699–703.

36 C. P. Gordon, C. Raynaud, R. A. Andersen, C. Copéret and O. Eisenstein, Carbon-13 NMR Chemical Shift: A Descriptor for Electronic Structure and Reactivity of Organometallic Compounds, *Accounts Chem Res*, 2019, 52, 2278–2289.

37 W. Rhim, D. D. Elleman and R. W. Vaughan, Analysis of multiple pulse NMR in solids, *J Chem Phys*, 1973, 59, 3740–3749.

38 R. Grosescu, A. M. A. (chmelnick), U. Haeberlen and H. W. Spiess, Multiple pulse study of the proton shielding in single crystals of maleic acid, *Chem Phys*, 1974, 5, 119–128.

39 F. A. Perras, U. Kanbur, A. L. Paterson, P. Chatterjee, I. I. Slowing and A. D. Sadow, Determining the Three-Dimensional Structures of Silica-Supported Metal Complexes from the Ground Up, *Inorg Chem*, 2022, 61, 1067–1078.

40 M. Adachi, C. Nédez, X. X. Wang, F. Bayard, V. Dufaud, F. Lefebvre and J.-M. Basset, Surface organometallic chemistry of zirconium Chemical reactivity of the ≡Si-O-$ZrNp_3$ surface complex synthesized on dehydroxylated silica and application to the modification of mordenite, *J Mol Catal Chem*, 2003, 204, 443–455.

41 J. Corker, F. Lefebvre, C. Lécuyer, V. Dufaud, F. Quignard, A. Choplin, J. Evans and J.-M. Basset, Catalytic Cleavage of the C-H and C-C Bonds of Alkanes by Surface Organometallic Chemistry: An EXAFS and IR Characterization of a Zr-H Catalyst, *Science*, 1996, 271, 966–969.

42 S. V. Dvinskikh, H. Zimmermann, A. Maliniak and D. Sandström, Measurements of motionally averaged heteronuclear dipolar couplings in MAS NMR using R-type recoupling, *J Magn Reson*, 2004, 168, 194–201.

43 A. Gansmüller, J.-P. Simorre and S. Hediger, Windowed R-PDLF recoupling: A flexible and reliable tool to characterize molecular dynamics, *J Magn Reson*, 2013, 234, 154–164.

44 X. Lu, H. Zhang, M. Lu, A. J. Vega, G. Hou and T. Polenova, Improving dipolar recoupling for site-specific structural and dynamics studies in biosolids NMR: windowed RN-symmetry sequences, *Phys Chem Chem Phys*, 2016, 18, 4035–4044.

45 X. Zhao, J. L. Sudmeier, W. W. Bachovchin and M. H. Levitt, Measurement of NH Bond Lengths by Fast Magic-Angle Spinning Solid-State NMR Spectroscopy: A New Method for the Quantification of Hydrogen Bonds, *J Am Chem Soc*, 2001, 123, 11097–11098.

46 J. S. Waugh, Sensitivity in Fourier transform NMR spectroscopy of slowly relaxing systems, *J Mol Spectrosc*, 1970, 35, 298–305.

47 G. Hou, X. Lu, A. J. Vega and T. Polenova, Accurate measurement of heteronuclear dipolar couplings by phase-alternating R-symmetry (PARS) sequences in magic angle spinning NMR spectroscopy, *J Chem Phys*, 2014, 141, 104202.

48 A. Brinkmann and M. H. Levitt, Symmetry principles in the nuclear magnetic resonance of spinning solids: Heteronuclear recoupling by generalized Hartmann–Hahn sequences, *J Chem Phys*, 2001, 115, 357–384.

49 M. Bak, J. T. Rasmussen and N. C. Nielsen, SIMPSON: A General Simulation Program for Solid-State NMR Spectroscopy, *J Magn Reson*, 2000, 147, 296–330.

50 T. Maly, G. T. Debelouchina, V. S. Bajaj, K.-N. Hu, C.-G. Joo, M. L. Mak–Jurkauskas, J. R. Sirigiri, P. C. A. van der Wel, J. Herzfeld, R. J. Temkin and R. G. Griffin, Dynamic nuclear polarization at high magnetic fields, *J Chem Phys*, 2008, 128, 052211.

51 A. Lesage, M. Lelli, D. Gajan, M. A. Caporini, V. Vitzthum, P. Miéville, J. Alauzun, A. Roussey, C. Thieuleux, A. Mehdi, G. Bodenhausen, C. Coperet and L. Emsley, Surface Enhanced NMR Spectroscopy by Dynamic Nuclear Polarization, *J Am Chem Soc*, 2010, 132, 15459–15461.

52 T. Kobayashi, F. A. Perras, I. I. Slowing, A. D. Sadow and M. Pruski, Dynamic Nuclear Polarization Solid-State NMR in Heterogeneous Catalysis Research, *ACS Catal*, 2015, 5, 7055–7062.

53 A. Zagdoun, G. Casano, O. Ouari, M. Schwarzwälder, A. J. Rossini, F. Aussenac, M. Yulikov, G. Jeschke, C. Copéret, A. Lesage, P. Tordo and L. Emsley, Large Molecular Weight Nitroxide Biradicals Providing Efficient Dynamic Nuclear Polarization at Temperatures up to 200 K, *J Am Chem Soc*, 2013, 135, 12790–12797.

54 G. Kontaxis, G. M. Clore and A. Bax, Evaluation of Cross-Correlation Effects and Measurement of One-Bond Couplings in Proteins with Short Transverse Relaxation Times, *J Magn Reson*, 2000, 143, 184–196.

55 J. H. Lee, J. Ying and A. Bax, Quantitative evaluation of positive ϕ angle propensity in flexible regions of proteins from three-bond *J* couplings, *Phys Chem Chem Phys*, 2015, 18, 5759–5770.

56 G. te Velde, F. M. Bickelhaupt, E. J. Baerends, C. F. Guerra, S. J. A. van Gisbergen, J. G. Snijders and T. Ziegler, Chemistry with ADF, *J Comput Chem*, 2001, 22, 931–967.

57 M. Ernzerhof and G. E. Scuseria, Assessment of the Perdew–Burke–Ernzerhof exchange-correlation functional, *J Chem Phys*, 1999, 110, 5029–5036.

58 M. Seth and T. Ziegler, Range-Separated Exchange Functionals with Slater-Type Functions, *J Chem Theory Comput*, 2012, 8, 901–907.

59 E. V. Lenthe and E. J. Baerends, Optimized Slater-type basis sets for the elements 1–118, *J Comput Chem*, 2003, 24, 1142–1156.

60 E. van Lenthe, E. J. Baerends and J. G. Snijders, Relativistic regular two-component Hamiltonians, *J Chem Phys*, 1993, 99, 4597–4610.

61 E. van Lenthe, E. J. Baerends and J. G. Snijders, Relativistic total energy using regular approximations, *J Chem Phys*, 1994, 101, 9783–9792.

62 E. van Lenthe, A. Ehlers and E.-J. Baerends, Geometry optimizations in the zero order regular approximation for relativistic effects, *J Chem Phys*, 1999, 110, 8943–8953.

63 E. van Lenthe, R. van Leeuwen, E. J. Baerends and J. G. Snijders, Relativistic regular two-component Hamiltonians, *Int J Quantum Chem*, 1996, 57, 281–293.

64 G. Schreckenbach and T. Ziegler, Calculation of NMR Shielding Tensors Using Gauge-Including Atomic Orbitals and Modern Density Functional Theory, *J Phys Chem*, 1995, 99, 606–611.

65 G. Schreckenbach and T. Ziegler, The calculation of NMR shielding tensors based on density functional theory and the frozen-core approximation, *Int J Quantum Chem*, 1996, 60, 753–766.

66 S. K. Wolff, T. Ziegler, E. van Lenthe and E. J. Baerends, Density functional calculations of nuclear magnetic shieldings using the zeroth-order regular approximation (ZORA) for relativistic effects: ZORA nuclear magnetic resonance, *J Chem Phys*, 1999, 110, 7689–7698.

67 M. Krykunov, T. Ziegler and E. van Lenthe, Hybrid density functional calculations of nuclear magnetic shieldings using Slater-type orbitals and the zeroth-order regular approximation, *Int J Quantum Chem*, 2009, 109, 1676–1683.

68 A. Comas-Vives, Amorphous SiO_2 surface models: energetics of the dehydroxylation process, strain, ab initio atomistic thermodynamics and IR spectroscopic signatures, *Phys Chem Chem Phys*, 2016, 18, 7475–7482.

69 P. Hohenberg and W. Kohn, Inhomogeneous Electron Gas, *Phys Rev*, 1964, 136, B864–B871.

70 W. Kohn and L. J. Sham, Self-consistent equations including exchange and correlation effects, *Phys. Rev.*, 1965, 140, A1133–A1138.

71 S. J. Clark, M. D. Segall, C. J. Pickard, P. J. Hasnip, M. I. J. Probert, K. Refson and M. C. Payne, First principles methods using CASTEP, *Zeitschrift Für Kristallographie - Cryst Mater*, 2005, 220, 567–570.

72 M. C. Payne, M. P. Teter, D. C. Allan, T. A. Arias and J. D. Joannopoulos, Iterative minimization techniques for ab initio total-energy calculations: molecular dynamics and conjugate gradients, *Rev Mod Phys*, 1992, 64, 1045–1097.

73 B. G. Pfrommer, M. Côté, S. G. Louie and M. L. Cohen, Relaxation of Crystals with the Quasi-Newton Method, *J Comput Phys*, 1997, 131, 233–240.

74 J. P. Perdew, K. Burke and M. Ernzerhof, Generalized Gradient Approximation Made Simple, *Phys Rev Lett*, 1996, 77, 3865–3868.

75 H. J. Monkhorst and J. D. Pack, Special points for Brillouin-zone integrations, *Phys Rev B*, 1976, 13, 5188–5192.

76 E. R. McNellis, J. Meyer and K. Reuter, Azobenzene at coinage metal surfaces: Role of dispersive van der Waals interactions, *Phys Rev B*, 2009, 80, 205414.

77 S. Grimme, Semiempirical GGA-type density functional constructed with a long-range dispersion correction, *J Comput Chem*, 2006, 27, 1787–1799.

78 S. Adiga, D. Aebi and D. L. Bryce, EFGShield A program for parsing and summarizing the results of electric field gradient and nuclear magnetic shielding tensor calculations, *Can J Chem*, 2007, 85, 496–505.

79 L. Zhang, J. Han, H. Wang, R. Car and W. E, Deep Potential Molecular Dynamics: A Scalable Model with the Accuracy of Quantum Mechanics, *Phys Rev Lett*, 2018, 120, 143001.

80 G. Kresse and J. Hafner, Ab initio molecular dynamics for liquid metals, *Phys Rev B*, 1993, 47, 558–561.

81 G. Kresse and J. Hafner, Ab initio molecular-dynamics simulation of the liquid-metal–amorphous-semiconductor transition in germanium, *Phys Rev B*, 1994, 49, 14251–14269.

82 G. Kresse and J. Furthmüller, Efficiency of ab-initio total energy calculations for metals and semiconductors using a plane-wave basis set, *Comp Mater Sci*, 1996, 6, 15–50.

83 G. Kresse and J. Furthmüller, Efficient iterative schemes for ab initio total-energy calculations using a plane-wave basis set, *Phys Rev B*, 1996, 54, 11169–11186.

84 D.-J. Liu and J. W. Evans, Reaction processes at step edges on S-decorated Cu(111) and Ag(111) surfaces: MD analysis utilizing machine learning derived potentials, *J Chem Phys*, 2022, 156, 204106.

85 F. Hoffmann, M. Cornelius, J. Morell and M. Fröba, Silica-Based Mesoporous Organic–Inorganic Hybrid Materials, *Angewandte Chemie Int Ed*, 2006, 45, 3216–3251.

86 S. S. Park, M. S. Moorthy and C.-S. Ha, Periodic mesoporous organosilicas for advanced applications, *Npg Asia Mater*, 2014, 6, e96–e96.

87 S. Bracco, A. Comotti, P. Valsesia, B. F. Chmelka and P. Sozzani, Molecular rotors in hierarchically ordered mesoporous organosilica frameworks, *Chem Commun*, 2008, 4798–4800.

88 A. D. Nicola, A. Correa, S. Bracco, J. Perego, P. Sozzani, A. Comotti and G. Milano, Collective dynamics of molecular rotors in periodic mesoporous organosilica: a combined solid-state ^{2}H-NMR and molecular dynamics simulation study, *Phys Chem Chem Phys*, 2021, 24, 666–673.

89 J. T. Damron, K. M. Kersten, M. K. Pandey, K. H. Mroue, J. R. Yarava, Y. Nishiyama, A. J. Matzger and A. Ramamoorthy, Electrostatic Constraints Assessed by ^{1}H MAS NMR Illuminate Differences in Crystalline Polymorphs, *J Phys Chem Lett*, 2017, 8, 4253–4257.

90 B. Berglund and R. W. Vaughan, Correlations between proton chemical shift tensors, deuterium quadrupole couplings, and bond distances for hydrogen bonds in solids, *J Chem Phys*, 1980, 73, 2037–2043.

91 S. Sorriso, Energy barrier to internal rotation in some ferrocene derivatives from dielectric measurements, *J Organomet Chem*, 1979, 179, 205–213.

92 W. D. Luke and A. Streitwieser, Barriers to ring rotation in 1,1',4,4'-tetra-tert-butyluranocene and 1,1',3,3'-tetra-tert-butylferrocene, *J Am Chem Soc*, 1981, 103, 3241–3243.

93 A. Kubo, R. Ikeda and D. Nakamura, Motion of C_5H_5 Rings in Three Crystalline Modifications of Ferrocene as Studied by 1H NMR, *Chem Lett*, 1981, 10, 1497–1500.

94 R. W. Schurko, I. Hung, S. Schauff, C. L. B. Macdonald and A. H. Cowley, Anisotropic ^{11}B and ^{13}C NMR Interaction Tensors in Decamethylcyclopentadienyl Boron Complexes, *J Phys Chem*, 2002, 106, 10096–10107.

95 R. Yu, S. Xu, M. Wang, T. Yang and Z. Cui, Metallocene: multi-layered molecular rotors, *Dalton T*, 2021, 50, 14156–14162.

96 T. Kobayashi, D. Singappuli-Arachchige, Z. Wang, I. I. Slowing and M. Pruski, Spatial distribution of organic functional groups supported on mesoporous silica nanoparticles: a study by conventional and DNP-enhanced ^{29}Si solid-state NMR, *Phys Chem Chem Phys*, 2016, 19, 1781–1789.

97 T. Kobayashi, I. I. Slowing and M. Pruski, Measuring Long-Range ^{13}C–^{13}C Correlations on a Surface under Natural Abundance Using Dynamic Nuclear Polarization-Enhanced Solid-State Nuclear Magnetic Resonance, *J Phys Chem C*, 2017, 121, 24687–24691.

98 T. Kobayashi, D. Singappuli-Arachchige, I. I. Slowing and M. Pruski, Spatial distribution of organic functional groups supported on mesoporous silica nanoparticles (2): a study by ^{1}H triple-quantum fast-MAS solid-state NMR, *Phys Chem Chem Phys*, 2018, 20, 22203–22209.

99 T. Kobayashi and M. Pruski, Spatial Distribution of Silica-Bound Catalytic Organic Functional Groups Can Now Be Revealed by Conventional and DNP-Enhanced Solid-State NMR Methods, *Acs Catal*, 2019, 9, 7238–7249.

100 J. C. C. Chan and R. Tycko, Recoupling of chemical shift anisotropies in solid-state NMR under high-speed magic-angle spinning and in uniformly ^{13}C-labeled systems, *J Chem Phys*, 2003, 118, 8378–8389.